JTTEE5 17:275–283
DOI: 10.1007/s11666-008-9169-1
1059-9630/$19.00 © ASM International



# Oxidation Control with Chromate Pretreatment of MCrAlY Unmelted Particle and Bond Coat in Thermal Barrier Systems

*Hideaki Yamano, Kazumi Tani, Yoshio Harada, and Takema Teratani*

*(Submitted August 31, 2007; in revised form December 12, 2007)*

**MCrAlY alloy bond coat is widely used in thermal barrier coating (TBC) systems to protect substrates from high-temperature oxidizing environments. However, failure of the ceramic topcoat can occur due to a thermally grown oxide (TGO) that grows at the interface between the bond coat and the topcoat. In this study, the effect of chromate treatment was investigated. Prior to topcoat deposition, a thin film of $Cr_2O_3$ was formed on the bond coat surface. High-temperature oxidation tests were carried out, and the oxidation rates were determined by inspection of cross sections. Similar oxidation tests were carried out using MCrAlY powder material assumed to be unmelted particles. As a result, the chromate-treated bond coat showed outstanding oxidation resistance. Calculations that take into account the oxidation of particles in the topcoat indicated the generation of internal stress to cause local fracture of the topcoat.**

**Keywords** chromate treatment, gas turbine, plasma spraying, thermal barrier coating, thermally grown oxide, unmelted particle

## 1. Introduction

As the operating temperature of a gas turbine has increased, development of heat-resistant alloy materials and heat-resistant coating has become an important theme in addition to demand for high efficiency of a cooling system, especially for hot-section parts such as burners, turbine blades, and vanes (Ref 1-4). Thermal barrier coating (TBC) systems, consisting of yttria partially stabilized zirconia (YSZ) topcoat and MCrAlX (M: Ni, Co, or their combinations; X: Y, Ce, La, and Hf) bond coat, have been widely used as thermal protective coating (Ref 5) since 1950s when their basic concept was built. However, delamination at the bond coat/topcoat interface occurs because of thermal stresses (Ref 6) or local stresses developed by the growth of thermally grown oxide (TGO) consisting of Co, Ni, Cr, and Al (Ref 7). Therefore, the development of a countermeasure against oxidation has become an important issue. Several studies have proposed growth-inhibiting methods for TGO, such as improvement of chemical compositions of MCrAlX alloy as a bond coat (Ref 8, 9), control of ambient during heat treatment of a bond coat (Ref 10), electron beam irradiation to a bond coat surface (Ref 11), and laser irradiation to a bond coat surface (Ref 12).

**Hideaki Yamano, Kazumi Tani, Yoshio Harada,** and **Takema Teratani**, Thermal Spraying Technology R&D Laboratory, Tocalo Co., Ltd., Akashi 674-0093, Japan. Contact e-mail: yamanohideak@tocalo.co.jp.

In our previous study, attention was focused on the wart-like oxide that grew as complex oxide near interface, and it was found that wart-like oxide generates cracks in the topcoat (Ref 10). In addition, it was reported that complex oxides may originate during the rapid oxidation of unmelted MCrAlY particles attached to the bond coat surface during spraying. Furthermore, to reduce the growth rate of oxides, the chromate treatment of the bond coat surface was suggested because the thin film of $Cr_2O_3$ promotes the growth of $Al_2O_3$ film, and it was reported that such $Al_2O_3$ film suppresses further growth of oxides (Ref 13).

In this study, the high-temperature oxidation behavior of the bond coat and the growth rate of the oxide are investigated. In addition, the effects of volume expansion due to oxidation of an unmelted particle near the topcoat/bond coat interface on the fracture of the $ZrO_2$ topcoat are discussed.

## 2. Experimental Procedure

### 2.1 Preparation of Samples

A Ni-based superalloy IN738LC polycrystalline material that is typical material for gas turbine blades was used as the substrate of sample ($50 \times 50 \times 5$ mm) for high-temperature oxidation test. After grit blasting of the substrate with $Al_2O_3$ grit, CoNiCrAlY alloy coating was formed by Low-Pressure Plasma Spraying (LPPS) as the bond coat (150 μm thick). The appearance of the bond coat surface is shown in Fig. 1. As shown in Fig. 1, numerous spherical particles were observed on the bond coat surface. These are considered to be the unmelted particles that did not pass through the high-temperature region of plasma jet during deposition. Following the bond

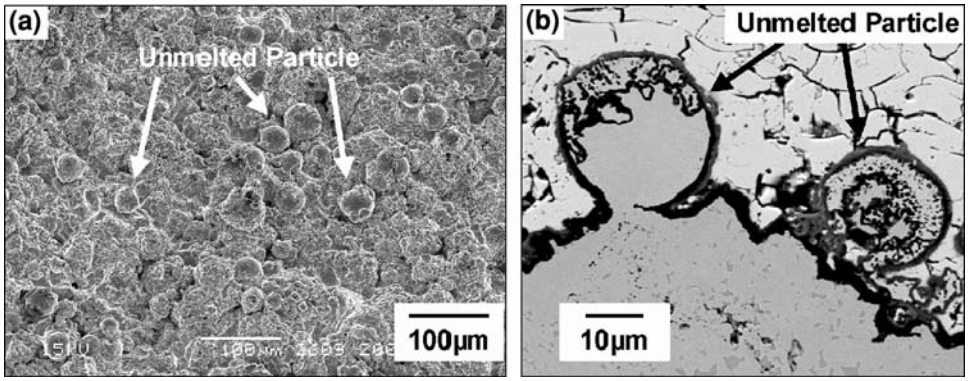


**Fig. 1** Unmelted particles on the bond coat surface: (a) coating surface after the bond coat deposition and (b) oxidized unmelted CoNiCrAlY particles in the topcoat

**Table 1 Chemical compositions of materials (wt.%)**

| | | | | | | | | | |
|---|---|---|---|---|---|---|---|---|---|
| Substrate | Ni | Cr | W | Mo | Co | Al | Ti | Ta | Nb |
| IN738LC | Bal. | 15.8 | 2.5 | 1.8 | 8.1 | 3.4 | 3.6 | 1.9 | 0.9 |
| Bond coat | Co | Ni | Cr | Al | Y | | | | |
| CoNiCrAlY | Bal. | 32.0 | 21.0 | 8.5 | 0.52 | | | | |
| Topcoat | Zr | Y | O | | | | | | |
| YSZ | 68.1 | 6.2 | 25.2 | | | | | | |

**Table 2 Spraying conditions**

| | LPPS | APS |
|---|---|---|
| Plasma gas | Ar, $H_2$ | Ar, $H_2$ |
| Power | 47 kW | 44 kW |
| Carrier gas | Ar | Ar |
| Powder feed rate | 20 g/min | 20 g/min |
| Spraying distance | 275 mm | 130 mm |
| Chamber pressure | 65 mbar | |

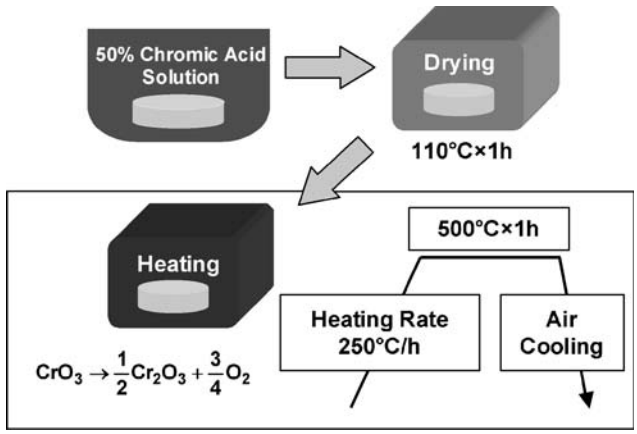


**Fig. 2** Chromate processing outline

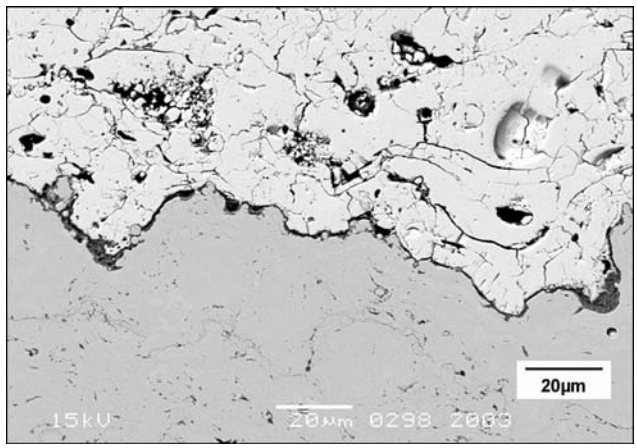


**Fig. 3** Cross-sectional micrograph of the TBC sample with the chromate treatment before oxidation test

coat deposition, 8 wt.% $Y_2O_3$-stabilized $ZrO_2$ (YSZ) coating was overlaid by Atmospheric Plasma Spraying (APS) as the topcoat (300 µm thick). The chemical compositions of the substrate and the coating materials are shown in Table 1. The spraying conditions are also shown in Table 2.

In addition to the common TBC samples described above, samples that had $Cr_2O_3$ layer applied at the bond coat/topcoat interface by chromate treatment were prepared. The schematic of the chromate process is shown in Fig. 2. After the bond coat deposition, the sample was (Ref 1) dipped into chromic acid anhydride ($CrO_3$) 50% solution, (Ref 2) dried at 110 °C for 1 h, and (Ref 3) heated at 500 °C for 1 h to form $Cr_2O_3$ thin film (0.1 µm thick) on the bond coat surface. Following the chromate treatment of the bond coat, the topcoat was overlaid similar to the common TBC sample. The cross-sectional micrograph of the TBC sample with the chromate treatment before oxidation test is shown in Fig. 3. From the micrograph, it is confirmed that the $Cr_2O_3$ film shown in light gray on the bond coat is very thin. However, it is also observed that thick $Cr_2O_3$ layers are formed around unmelted particles and at concave parts on the bond coat surface. These thick layers seem to be formed because

puddles of $CrO_3$ solution exist at such locations during firing process.

### 2.2 High-Temperature Oxidation Test

Using both the TBC samples with and without the chromate treatment, high-temperature oxidation tests at 1150 °C in air were carried out. The dwell times were set at 4, 9, and 25 h. After the high-temperature oxidation tests, cross sections of the samples were observed by a scanning electron microscope (SEM: JEOL Ltd., JSM-5600LV) and analyzed by an electron probe microanalyzer (EPMA: OXFORD INSTRUMENTS, INCA Energy), and the differences in oxidation behavior between the TBC samples with and without the chromate treatment were investigated. Additionally, growth rate of each oxide layer was determined, and the effect of the chromate treatment against interfacial oxidation was confirmed quantitatively. Similar oxidation tests were also carried out using MCrAlY powder material samples, and the effect of the chromate treatment against the unmelted particles was investigated.

## 3. Results and Discussions

### 3.1 Effects of Chromate Treatment on Interfacial Oxidation

The cross-sectional micrograph of the TBC sample without the chromate treatment tested at 1150 °C for 4 h is shown in Fig. 4. In this figure, it was observed that TGO consisted of two kinds of oxides, the continuous oxide layer along the bond coat/topcoat interface and the wart-like oxide. The wart-like oxides were often observed at the part that the bond coat protruded into the topcoat. Such oxide is considered to originate in an unmelted particle attached to the bond coat surface without flattening during the bond coat deposition, and the unmelted particle seems to change into the wart-like oxide due to its rapid oxidation (Ref 10, 14). Also, at the part that such wart-like oxides grew, the continuous and dense oxide layer was interrupted. Therefore, such part seems to have a low oxidation protection and tends to be oxidized selectively. These local rapid oxidations at the part that the bond coat protruded into the topcoat may generate local internal stresses near the bond coat/topcoat interface, and these can cause local fracture of the topcoat (Ref 10, 15).

The element distributions near the interface of the TBC sample without the chromate treatment tested at 1150 °C for 25 h are shown in Fig. 5. As shown in this figure, the continuous oxide layer along the interface consists of $Al_2O_3$ and hardly includes other metal elements. However, the wart-like oxide includes all metal elements of Co, Ni, Cr, and Al, and it is considered to be their complex oxide.

On the other hand, the different oxidation behavior from the common TBC samples was observed in the case that the chromate treatment was applied to the bond coat surface. The cross-sectional micrograph of the TBC sample with the chromate treatment tested at 1150 °C for 4 h is shown in Fig. 6. In this figure, the wart-like oxide was not observed even at the part that the bond coat protruded into the topcoat, and the continuous oxide layer had grown at the protrusion. As a result, it was observed that almost all the bond coat surface was covered by the protective oxide layer. In addition, there were smaller amounts of unmelted particles on the chromate-treated bond coat surface. That is because the unmelted particles have weak adhesion to the bond coat surface, and they were easily removed during the chromate treatment. The effect of the chromate treatment is also apparent at the protrusions of the bond coat surface that were formed as stacks of melted particles onto an unmelted particle. From the cross-sectional micrograph of the sample after oxidation test, oxides shown in light gray appear to have grown relatively thick around small unmelted particles and at concave parts on the bond coat surface. However, these oxides consist of $Cr_2O_3$ formed by the chromate treatment, and they had already existed when the topcoat deposition started. Therefore, they do not change during high-temperature oxidation and never generate local stresses near the interface.

The element distributions near the interface of the TBC sample with the chromate treatment tested at 1150 °C for 25 h are shown in Fig. 7. From these results, it was confirmed that all oxides formed by high-temperature oxidation test consist of $Al_2O_3$ layer and that the oxides shown in light gray consist of $Cr_2O_3$ layer only.

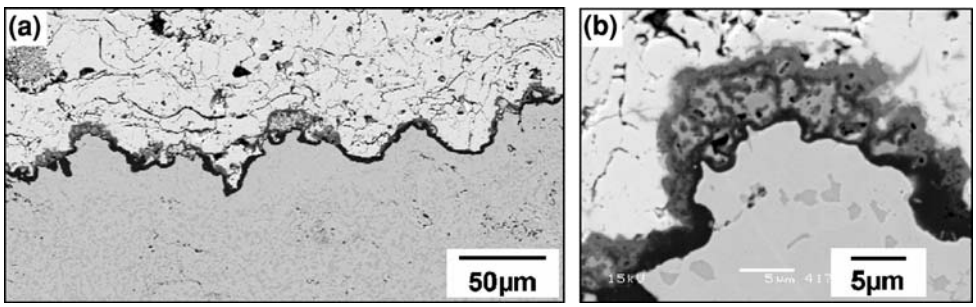


**Fig. 4** Cross-sectional micrographs of interface after high-temperature exposure test (1150 °C, 4 h) without chromate pretreatment: (a) two kinds of TGO grew at the interface and (b) oxidized unmelted CoNiCrAlY particle

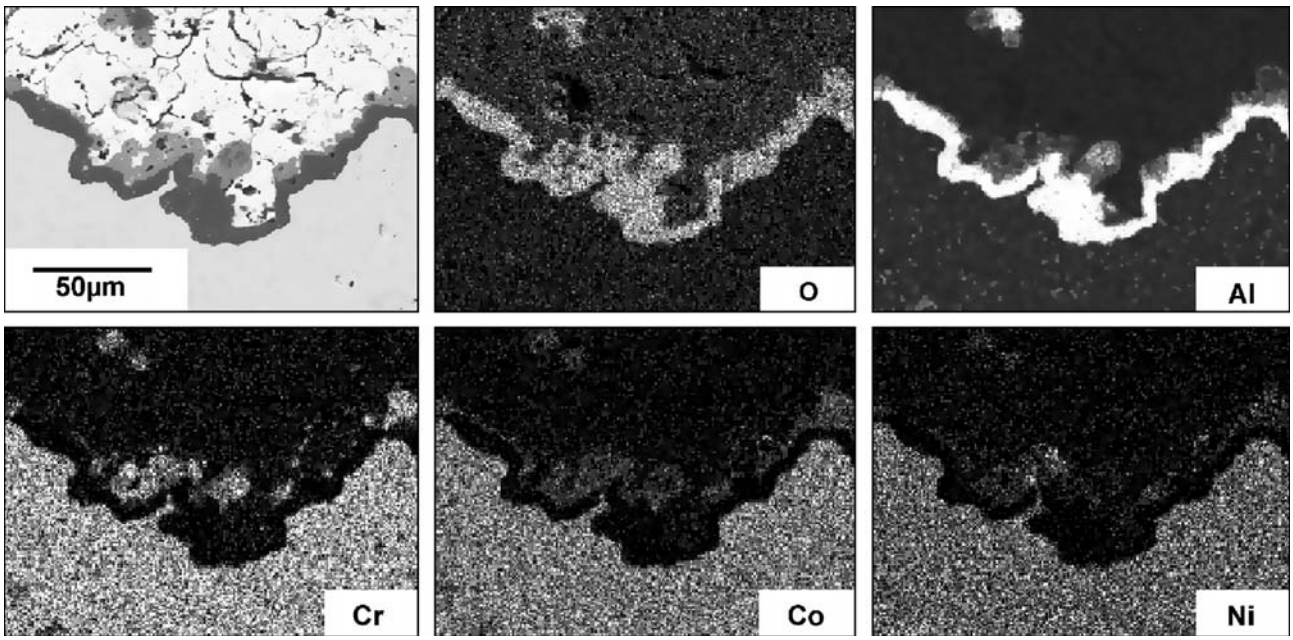


**Fig. 5** EPMA results of interface after high-temperature exposure test (1150 °C, 25 h) without chromate pretreatment

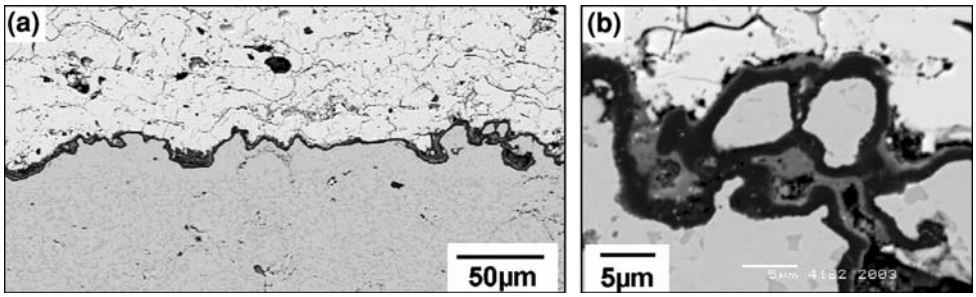


**Fig. 6** Cross-sectional micrographs of interface after high-temperature exposure test (1150 °C, 4 h) with chromate pretreatment: (a) the bond coat surface was covered by continuous $Al_2O_3$ layer and (b) unmelted CoNiCrAlY particles were also protected by an oxidation-resistant $Al_2O_3$ layer

Because $Al_2O_3$ layer is formed due to internal oxidation and grows inward (Ref 16), it is observed that the $Al_2O_3$ layer exists below the $Cr_2O_3$ layer preformed by chromate treatment. The wart-like oxides were hardly observed.

The oxidation rates of the TBC samples both with and without the chromate treatment are shown in Fig. 8. The thicknesses are average values of 10 data measured from each sample with the exception of the wart-like oxides. In this work, assuming the growth of the oxide layer to obey the parabolic law, the horizontal axis shows the square root of oxidation time. From these results, it was found that the gradient of the approximation line of the TBC sample with the chromate treatment was smaller than that of the sample without the treatment by a factor of four, and it was confirmed quantitatively that the oxidation of the bond coat surface is suppressed remarkably by the chromate treatment.

### 3.2 Effects of Chromate Treatment on Oxidation of Unmelted Particles

To confirm the effects of the chromate treatment on the oxidation of unmelted particles in detail, assuming the CoNiCrAlY powder materials to be the unmelted particles, high-temperature oxidation tests of the CoNiCrAlY powder materials at 1150 °C for 9 h were carried out. The cross-sectional micrographs after the oxidation tests of the CoNiCrAlY powder materials with and without the chromate treatment are shown in Fig. 9.

From these results, it is apparent that the oxidation behavior of the powder sample with the chromate treatment was quite different from that of the powder sample without the chromate treatment. In the micrograph of the sample without the treatment, a large amount of oxides shown in light gray were seen, and the small particles were oxidized completely inward. These appearances are

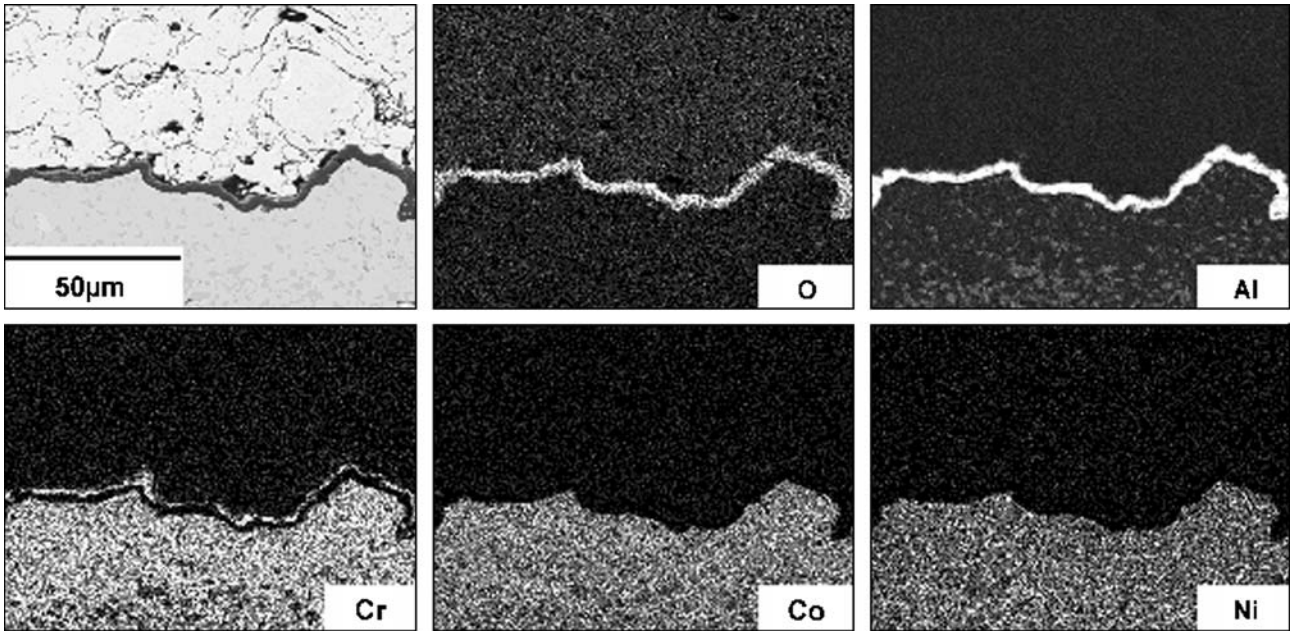


**Fig. 7** EPMA results of interface after high-temperature exposure test (1150 °C, 25 h) with chromate pretreatment

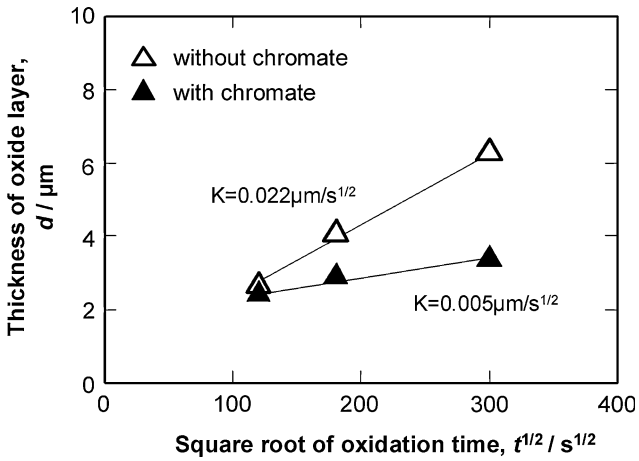


**Fig. 8** Oxidation rates of bond coat surface with and without chromate pretreatment

similar to the wart-like oxides observed in the TBC samples after the oxidation tests. On the other hand, the oxides of the powder sample with the treatment had grown only on the surface of the particles, and their inner side had remained at metal phase.

The element distributions of the powder sample without the chromate treatment after the oxidation test are shown in Fig. 10. The protective oxide layer that consisted of $Al_2O_3$ had grown on a surface of relatively large particles; however, such oxide layer had never been seen in small particles. Also, it seemed that fully oxidized small particles consisted of a complex oxide in the entire particle; thus, it is considered that the unmelted particles on the bond coat tend to change into the wart-like oxides observed in the TBC samples after the oxidation tests.

The element distributions of the powder sample with the chromate treatment after the oxidation test are shown in Fig. 11. From these results, it was found that the

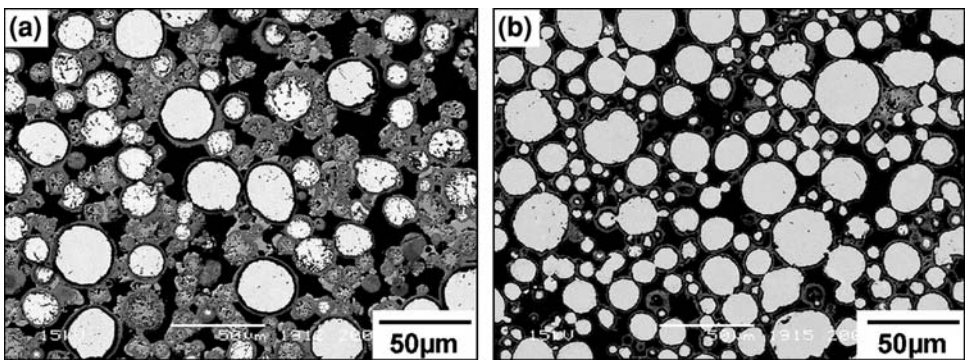


**Fig. 9** Oxidation behavior of CoNiCrAlY particles after high-temperature exposure test (1150 °C, 9 h): (a) without chromate pretreatment and (b) with chromate pretreatment

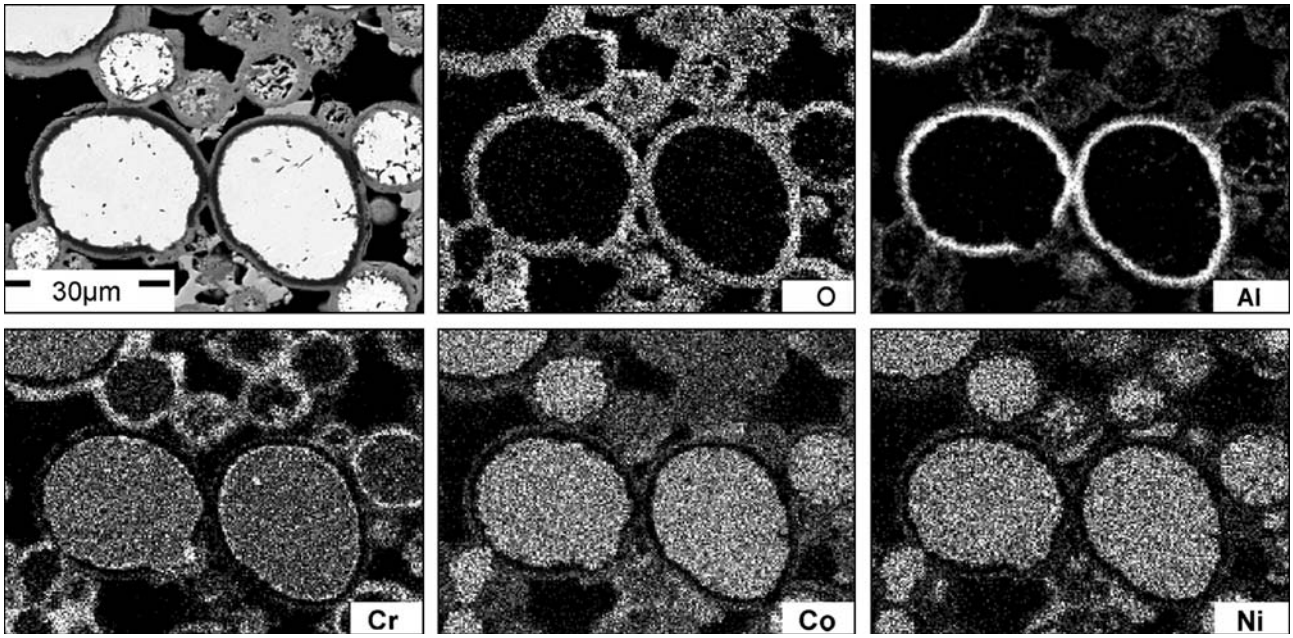


**Fig. 10** EPMA results of CoNiCrAlY particles after high-temperature exposure test (1150 °C, 9 h) without chromate pretreatment

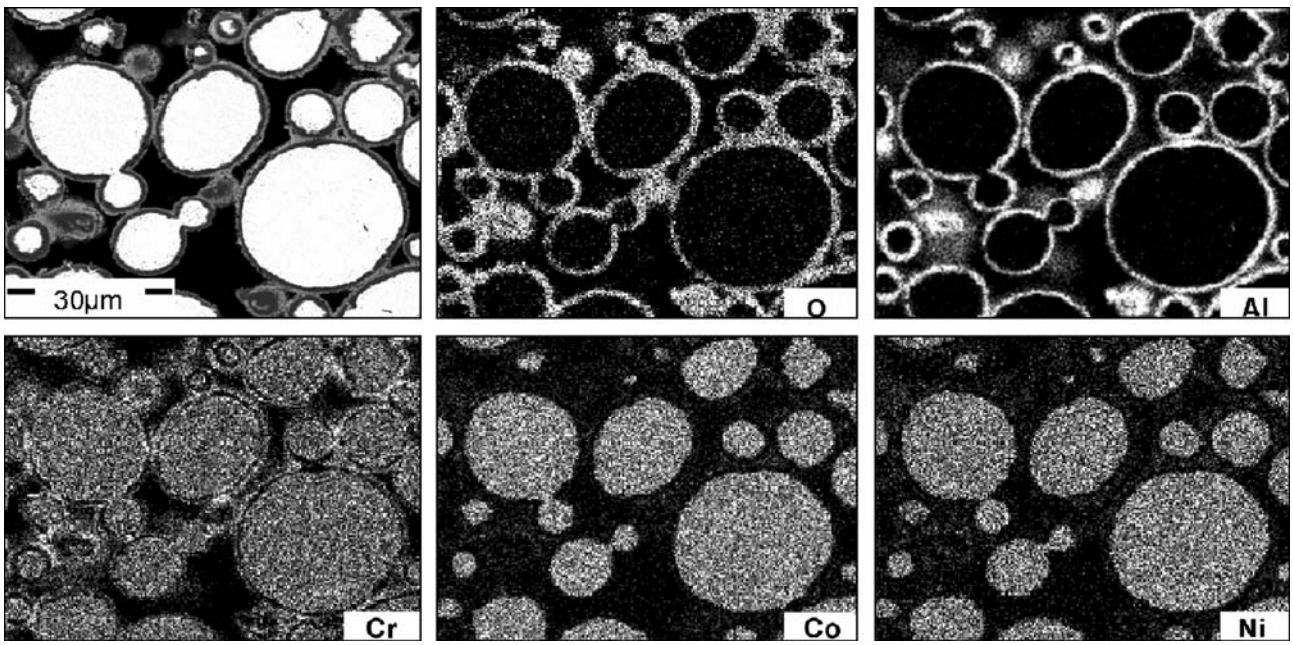


**Fig. 11** EPMA results of CoNiCrAlY particles after high-temperature exposure test (1150 °C, 9 h) with chromate pretreatment

protective oxide layer had grown even on small particles during high-temperature oxidation. By comparing it with the result of the powder sample without the chromate treatment, it is apparent that such protective $Al_2O_3$ layer suppresses further oxidation.

From the results of the oxidation tests, the chromate treatment is thought to be quite useful as a countermeasure against the oxidation of the bond coat surface and unmelted particles.

### 3.3 Oxidation Inhibition Mechanism by Chromate Treatment

Considering the Gibbs free-energy change accompanied with the oxidation of metal elements that compose the CoNiCrAlY alloy, as shown in Table 3, the standard free energy of oxide formation of Al has the largest absolute value of negative value except for that of Y that is included with a low content (0.52 wt.%). Therefore,

**Table 3 Free-energy changes associated with reduction of $Cr_2O_3$**

| Reaction | ΔG at 1150 °C |
|---|---|
| $Cr_2O_3 + 2Al \rightarrow Al_2O_3 + 2Cr$ | –445 kJ/mol |
| $Cr_2O_3 + 3Co \rightarrow 3CoO + 2Cr$ | +300 kJ/mol |
| $Cr_2O_3 + 3Ni \rightarrow 3NiO + 2Cr$ | +368 kJ/mol |

$Al_2O_3$ is expected to grow preferentially during oxidation process of CoNiCrAlY alloy.

However, $ZrO_2$ topcoat has less ability as oxygen barrier for the bond coat surface under high-temperature environment because of the existence of oxygen diffusion paths such as microcracks and open pores, and high oxygen ion conductivity at high temperatures that is characteristic of a stabilized $ZrO_2$ (Ref 17). At the early stage of oxidation under such high enough oxygen partial pressure, the complex oxides grow rapidly by simultaneous oxidation of all metal elements at the bond coat surface, especially protrusion parts. In addition, the promotion of local oxidation leads to the development of local stresses near the bond coat/topcoat interface.

On the other hand, in the case that $Cr_2O_3$ thin film was formed on the bond coat surface by the chromate treatment, the oxidation inhibition mechanisms are considered as described below.

(1) The $Cr_2O_3$ thin film plays a role as oxygen diffusion barrier and promotes the selective growth of $Al_2O_3$ due to reduction of oxygen partial pressure below the $Cr_2O_3$ film. If the oxygen partial pressure at the bond coat alloy surface can be reduced below the equilibrium dissociation oxygen partial pressures of CoO and NiO, Co and Ni cannot be oxidized thermodynamically. From basic calculations in thermodynamics, the equilibrium dissociation oxygen partial pressures at 1000 °C are calculated to be $1.7 \times 10^{-10}$ atm of NiO, $1.6 \times 10^{-12}$ atm of CoO, $2.5 \times 10^{-22}$ atm of $Cr_2O_3$, and $1.3 \times 10^{-35}$ atm of $Al_2O_3$.

(2) In addition to the role as oxygen diffusion barrier, the $Cr_2O_3$ thin film promotes the selective growth of $Al_2O_3$ because only Al element can reduce $Cr_2O_3$ and oxidize Al element itself, as shown in Table 3.

However, further detailed investigations are required to clarify the mechanisms of oxidation inhibition by application of $Cr_2O_3$ thin film on the bond coat.

### 3.4 Local Stress Around Oxidized Unmelted Particle in Topcoat

To verify the effect of the oxidation of the unmelted particle on local fracture of the topcoat, local stresses due to volume expansion of an oxidizing particle in the topcoat were calculated using mechanical models. In these calculations, both the topcoat and the oxide particle of CoNiCrAlY were assumed to be continuous and elastic material. Effects of other stress components, such as thermal stress, quenching stress during deposition, and so on, and effects of the topcoat/bond coat interface near the oxidizing particle were ignored.

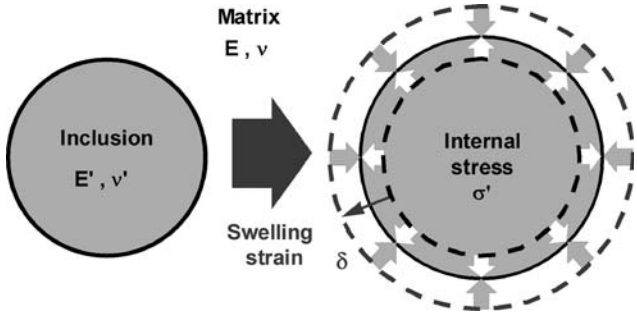


**Fig. 12** Model for calculation of internal stress due to oxidation

**Table 4 Pilling-Bedworth ratio**

| System | PB ratio |
|---|---|
| Co/CoO | 1.99 |
| Ni/NiO | 1.52 |
| $Cr/Cr_2O_3$ | 1.99 |
| $Al/Al_2O_3$ | 1.28 |

Using the model of the equivalent inclusion method by Eshelby (Ref 18), the stress that is developed in the complex oxide particle during its oxidation was calculated. The schematic of the model is shown in Fig. 12. Considering the continuity of normal stress in a direction perpendicular to the particle/topcoat interface and displacement at the interface without any fracture, the stress $\sigma'$ in the particle due to oxidation is given by

$$\sigma' = -\frac{2EE'}{2(1-2\nu')E + (1+\nu)E'} \cdot \delta \qquad \text{(Eq 1)}$$

where $\delta$ is the swelling strain of the particle due to oxidation without external constraint, $E$ and $\nu$ are Young's modulus and Poisson's ratio of the topcoat, $E'$ and $\nu'$ are Young's modulus and Poisson's ratio of the complex oxide particle, respectively. The swelling strain due to oxidation was determined as follows. Assuming CoNiCrAlY alloy consists of four elements of Co, Ni, Cr, and Al, the Pilling-Bedworth ratio (PB ratio) (Ref 19) of CoNiCrAlY alloy of 1.7 was determined by the PB ratios shown in Table 4 and volume fractions of each element. Then, the PB ratio of 1.7 was converted to the one-dimensional swelling strain $\delta$ of 0.20. This free expansion strain is caused by material change accompanied with addition of O element and is much larger than strains of usual material deformation (e.g., thermal expansion).

The calculated stress in the oxide particle as a function of Young's modulus is shown in Fig. 13. From these results, it is confirmed that the large swelling strain due to oxidation can generate remarkably large compressive stress in the oxide particle even if Young's modulus of the oxide is small. Such large compressive stress generates large tensile hoop stress in the topcoat near the particle/topcoat interface and can lead to local fracture of the

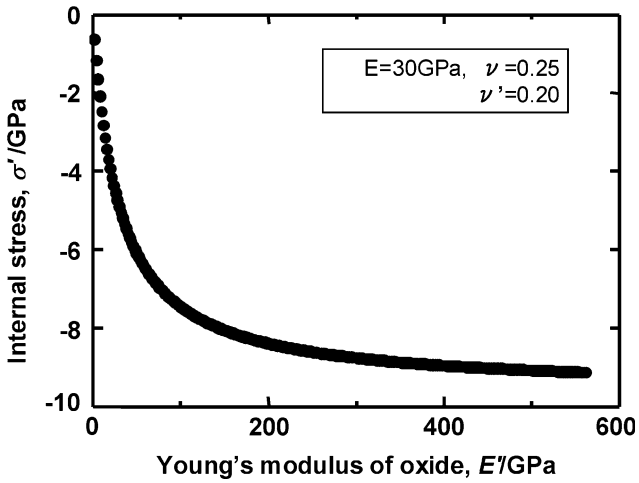


**Fig. 13** Stress generated in the fully oxidized particle as a function of Young's modulus of the oxide particle

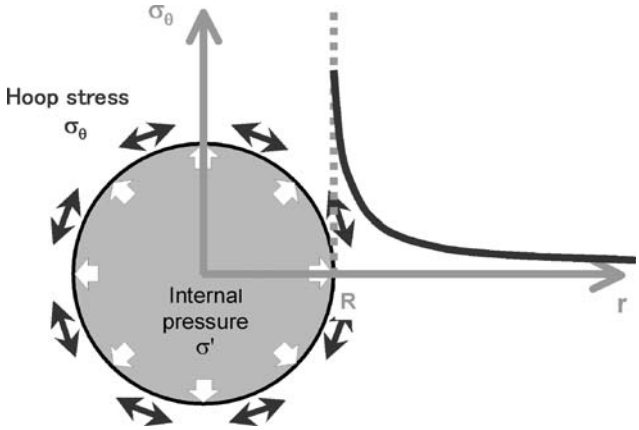


**Fig. 14** Model for calculation of stress distribution in the topcoat due to oxidation

topcoat. Therefore, the stress distribution in the topcoat around the oxide particle was also calculated. The schematic of the model is shown in Fig. 14. Using a spherically symmetric mechanical model, the hoop stress $\sigma_\theta$ in the topcoat around the oxide particle is given by

$$\sigma_\theta = -\frac{1}{2}\left(\frac{R}{r}\right)^3 \sigma' \quad (r > R) \qquad \text{(Eq 2)}$$

where $r$ is the distance from the center of the oxide particle, $R$ is the radius of the oxide particle, $\sigma'$ is the stress in the oxide particle. The hoop stress distribution in the topcoat is shown in Fig. 15. It is found that the hoop stress in the topcoat shows the maximum value of $0.5|\sigma'|$ at the particle/topcoat interface and diminishes drastically with distance from the oxide particle. The stress distribution will change after radial cracking (Ref 10, 15) occurs at the particle/topcoat interface, and the crack may extend by stress concentration at the crack tip. Thus, the range of topcoat fractures cannot be estimated from this result. However, even if such cracks cannot extend enough to

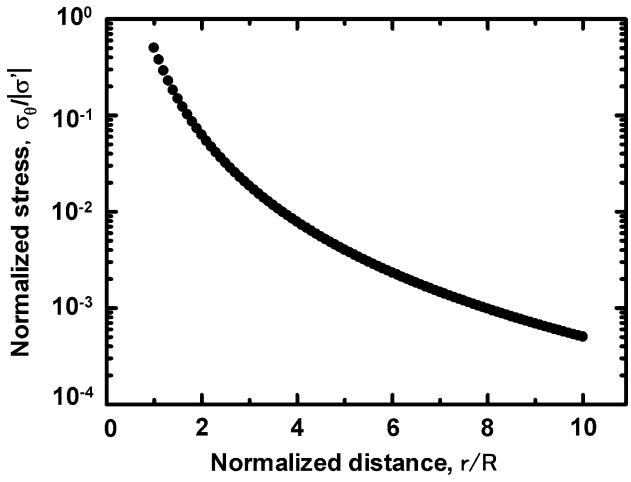


**Fig. 15** Normalized stress distribution in the topcoat as a function of normalized distance from the center of the oxide particle

spall the entire topcoat, they can be the origin of large cracks when additional loads such as external load and thermal load will be applied. Therefore, to improve the life of TBC, it is essential not to retain the unmelted particles that tend to change rapidly into the complex oxides on the bond coat surface. On the other hand, during spraying, the thermal histories of each flight particle of powder material are different from each other depending on each diameter and each trajectory in the plasma jet. Thus, in practice, it is impossible to deposit the coating without unmelted particles. Therefore, instead of removing the unmelted particles, the chemical treatment to not oxidize them rapidly is considered to be an effective countermeasure against this problem.

## 4. Conclusions

(1) $Cr_2O_3$ thin film on the bond coat formed by the chromate treatment promotes the growth of a protective $Al_2O_3$ layer on the bond coat surface, including unmelted particles, in the early stage of oxidation and suppresses further oxidation.

(2) Unmelted particles on the bond coat tend to be oxidized preferentially as complex oxide and can cause the cracking of the topcoat around the particle because oxidation is accompanied with large volume expansion.

(3) The application of $Cr_2O_3$ film on the bond coat by the chromate treatment is effective as a countermeasure against the oxidation problem of TBC systems.

### References

1. Heat Transfer and Cooling in Gas Turbines, T. Arts, Ed., Lecture Series 1995-05. Waterloo, Belgium: von Karman Institute for Fluid Dynamics, 1995

2. High Temperature Gas Turbines and Cooling Systems, Report of the 21st research Committee, Gas Turbine Society of Japan, Tokyo, 1997
3. N. Mifune and Y. Harada, Mechanism of Vertical Microcracking in $CaO{\cdot}SiO_2$-$CaO{\cdot}ZrO_2$ Sprayed Thermal Barrier Top Coating, *Mater. Trans.*, 2004, **45**, p 1788-1793
4. M. Okazaki, I. Ohtera, Y. Harada, and K. Namba, Undesirable Effect of Local Cellular Transformation in Microstructurally-Controlled Ni-base Superalloys Subjected to Previous Damage on High Temperature Fatigue Strength and the Prevention: For Recoating and Refurbishment Technology, *Mater. Sci. Res. Int.*, 2003, **9**, p 55-60
5. R. Miller, Current Status of Thermal Barrier Coatings – An Overview, *Surf. Coat. Technol.*, 1987, **30**, p 1-11
6. G. Chang, W. Phucharoen, and R. Miller, Behavior of Thermal Barrier Coatings for Advanced Gas Turbine Blades, *Surf. Coat. Technol.*, 1987, **30**, p 13-28
7. M. Okazaki, The Potential for the Improvement of High Performance Thermal Barrier Coatings, *Mater. Sci. Res. Int.*, 2003, **9**, p 3-8
8. T. Kato, K. Ogawa, and T. Shoji, Development of Thermal Barrier Coatings for Enhancement of Delamination Resistant Property, *J. Jpn. Therm. Spray. Soc.*, 2002, **39**, p 52-57, (in Japanese)
9. K. Ogawa, K. Ito, T. Shoji, D.W. Seo, H. Tezuka, and H. Kato, Effects of Ce and Si Additions to CoNiCrAlY Bond Coat Materials on Oxidation Behavior and Crack Propagation of Thermal Barrier Coatings, *J. Therm. Spray Technol.*, 2006, **15**(4), p 640-651
10. S. Takahashi, M. Yoshiba, and Y. Harada, Nano-Characterization of Ceramic Top-Coat/Metallic Bond-Coat Interface for Thermal Barrier Coating Systems by Plasma Spraying, *Mater. Trans.*, 2003, **44**, p 1181-1189
11. D. Strauss, G. Müller, G. Schumacher, V. Engelko, W. Stamm D. Clemens, and W.J. Quaddakers, Oxide Scale Growth on MCrAlY Bond Coatings After Pulsed Electron Beam Treatment and Deposition of EBPVD-TBC, *Surf. Coat. Technol.*, 2001, **135**, p 196-201
12. M. Tanno, K. Ogawa, T. Shoji, S.O. Chwa, and A. Ohmori, Bond Strength Improvement of Thermal Barrier Coatings by Laser Remelting Process, *J. Jpn. Therm Spray. Soc.*, 2003, **40**, p 159-165, (in Japanese)
13. T. Teratani, T. Suizu, K. Tani, and Y. Harada, Formation of Alumina Protective Layer on MCrAlY Atmospheric Plasma Sprayed Coating by Chromate Processing, *J. High Temp. Soc.*, 2003, **29**(Supplement), p 247-252, (in Japanese)
14. S. Takahashi, M. Yoshiba, and Y. Harada, Influence of Coating Process on High-Temperature Oxidation Property for Plasma Sprayed Thermal Barrier Coating Systems, *J. Jpn. Inst. Met.*, 2004, **68**, p 438-446, (in Japanese)
15. M. Nanko, M. Yoshimura, and T. Maruyama, High Temperature Oxidation of $Y_2O_3$ Partially-Stabilized $ZrO_2$ Composites Dispersed with Ni Particles, *Mater. Trans.*, 2003, **44**, p 736-742
16. J.K. Tien and F.S. Pettit, Mechanism of Oxide Adherence on Fe-25Cr-Al(Y or Sc) Alloys, *Metall. Trans.*, 1972, **3**(6), p 1587-1599
17. J.F. Baumard and P. Abelard, Advances in Ceramics, Vol. 12, *Science and Technology of Zirconia II*, N. Claussen, M. Ruhle, and A.H. Heuer, Eds., Columbus, OH: American Ceramic Society, 1984, p 555
18. J. Eshelby, The Determination of the Elastic Field of an Ellipsoidal Inclusion, and Related Problems, *Proc. Roy. Soc. Lond. Ser. A*, 1957, **A241**, p 376-396
19. N. Pilling and R. Bedworth, The Oxidation of Metals in High Temperature, *J. Inst. Met.*, 1923, **29**, p 529-591